Rapid Monitoring of Oxygenation by [19]F Magnetic Resonance Imaging: Simultaneous Comparison with Fluorescence Quenching

Bénédicte F. Jordan,[1,2] Greg O. Cron,[1,3] and Bernard Gallez[1,2]*

The aim of this study was to develop an MRI fluorocarbon oximetry technique using snapshot inversion recovery and compare it with fluorescence quenching fiber-optic probe oximetry (OxyLite) performed simultaneously in experimental mouse tumors. The oxygen reporter probe hexafluorobenzene (HFB) was injected directly into the tumors, along with the insertion of the OxyLite probe. Tumor oxygenation (pO$_2$) was modified using carbogen or lethal doses of the anesthetic gas. MRI pO$_2$ maps were generated in 1.5 min with an in-plane spatial resolution of 1.88 mm. MRI and OxyLite showed consistent baseline and postmortem pO$_2$ values. Increases in tumor pO$_2$ during carbogen breathing showed similar kinetics for the two methods. The pO$_2$ values observed using the OxyLite corresponded with relatively hypoxic values observed by MRI. The apparent discrepancy between mean values might be due to the difference in sampling volumes of the techniques and the observation of multiple locations using ^{19}F MRI versus a single location using the large optical fiber. Overall, the present method provides a rapid way to map the tumor oxygenation and is particularly suitable to monitor acute changes of pO$_2$ in tumors. Magn Reson Med 61:634–638, 2009. © 2008 Wiley-Liss, Inc.

Key words: hypoxia; OxyLite; ^{19}F MRI; fluorescence quenching

Hypoxia is a characteristic feature of locally advanced solid tumors resulting from an imbalance between oxygen supply and consumption (1). The role of hypoxia in increasing tumor resistance to radiation therapy has been well established (2). More recently, tumor hypoxia has been shown to decrease the efficacy of certain cytotoxic drugs (3,4). Moreover, investigations conducted over the past two decades have demonstrated that tumor hypoxia, in addition to diminishing therapeutic efficacy, plays a pivotal role in malignant progression. Methods to determine tumor oxygenation are therefore of crucial importance for the prediction of therapeutic outcome. Among the numerous techniques considered to increase temporarily intratumoral oxygenation for therapeutic advantage in experimental tumors (5,6), few have been tested in the clinical setting. This might be due to the lack of methods available to monitor dynamically and noninvasively tumor oxygenation in humans. Many current methods, such

as Eppendorf electrodes, near infrared spectroscopy, hypoxia reporter agents, and susceptibility NMR-based methods are either highly invasive, nonquantitative, or lack spatial resolution. An emerging method to dynamically map tumor oxygenation is electron paramagnetic resonance (EPR) imaging. MRI methods, however, are still more widely available and ^{19}F MRI oximetry methods have shown their potential utility. Mason and colleagues (7) have been successfully developing FREDOM MRI (fluorocarbon relaxometry using echo planar imaging for dynamic oxygen mapping) following direct intratumoral injection of the oxygen reporter molecule hexafluorobenzene (HFB). The technique was used to study tumor oxygenation after chemotherapy and radiotherapy and was compared with near-infrared spectroscopy (NIRS), fiber optic probes, oxygen needle electrodes, and the hypoxia marker pimonidazole (8–11). The aim of the current study was to develop an MRI fluorocarbon relaxometry technique (similar to Mason's FREDOM) to measure tumor oxygenation and compare it with simultaneous measurements from an MR-compatible fiber-optic probe.

MATERIALS AND METHODS

Tumor Model and Experimental Protocol

A transplantable liver tumor model (TLT) (12) was implanted in the leg of NMRI mice. For inoculation, ≈10^6 cells in 0.1 mL of media were injected intramuscularly into the right leg. Mice developed palpable tumors within a week of inoculation. Tumors were allowed to grow to 8 mm in diameter prior to experimentation. Animals were anesthetized by inhalation of isoflurane mixed with 21% oxygen (air) in a continuous flow (1.5 L/h), delivered by a nose cone. Anesthesia was induced using 3% isoflurane. It was then stabilized at 1.8% for a minimum of 15 min before any measurement. Warm air was flushed into the magnet in order to maintain normothermia. All experiments were conducted according to national animal care regulations. After induction and stabilization of anesthesia, baseline measurements were acquired under air-breathing conditions for 10 min. Subsequently, air was switched to carbogen (95% O$_2$, 5% CO$_2$) for 50 min. Finally, the mouse was sacrificed using 5% isoflurane in air for 20 min.

pO$_2$ Measurements

[19]F MRI Measurements

MRI was performed with a 4.7T (200 MHz, ^{1}H), 40 cm inner diameter bore system (Bruker Biospec, Ettlingen,

Germany). A tunable ^{1}H/^{19}F surface coil was used for RF transmission and reception.

Parametric images of the spin-lattice relaxation time (T_1) were estimated using a snapshot inversion recovery (SNAP-IR) pulse sequence (13–15). The pulse sequence consisted of a nonselective hyperbolic secant inversion pulse (10 ms length), followed by acquisition of a series of 512 rapid gradient echo images (repetition time = 10.9 ms, echo time = 4.2 ms, flip angle = 1°, matrix = 32 × 16, field of view = 60 × 30 mm, bandwidth = 12.5 kHz, single thick slice [projection], total acquisition time = 1.5 min) (Fig. 1). Raw (k-space) data were zero-filled to a matrix size of 64 × 64, resulting in interpolated 64 × 64 images. For each image pixel T_1 was estimated by fitting the standard 3-parameter monoexponential recovery equation (magnitude data only) describing the signal as a function of inversion time (13–15). We denote this computed T_1 as T_1' because the recovery curve is somewhat perturbed by the RF pulses (16). We then computed $R_1' = 1/T_1'$.

Calibration of HFB (R_1' with respect to pO_2) was performed by measuring R_1' in three different sealed tubes containing 300 μL HFB respectively bubbled with nitrogen (0% O_2 = 0 mmHg), air (21% O_2 = 160 mmHg), and carbogen (95% O_2 = 722 mmHg) for 20 min in a 37° water bath before measurement.

For in vivo studies, HFB was injected into the tumor via an insulin syringe (29G) and deposited along three tracks (3 × 30 μL) encompassing both central and peripheral regions in a coronal plane. HFB was deoxygenated by bubbling nitrogen for 5 min before use (10). MRI scout images were obtained for both ^{1}H (200.1 MHz) and ^{19}F (188.3 MHz) to reveal HFB distribution within the tumor. SNAP-IR images were used to measure pO_2 while mice breathed air, then carbogen, then isoflurane 5% in air.

Fluorescence Quenching Measurements

We used the OxyLite (Oxford Optronix, Oxford, UK) system for continuously monitoring tumor oxygenation and temperature simultaneously with ^{19}F MRI. An MR-compatible fiber-optic microprobe was inserted into the tumor (under the MR surface coil). The probe was inserted longitudinally into the middle of the tumor, parallel to the plane of the surface coil. This microprobe consisted of a thermocouple and an oxygen sensor based on the fluorescence quenching of a platinum-based fluorophore. Probes
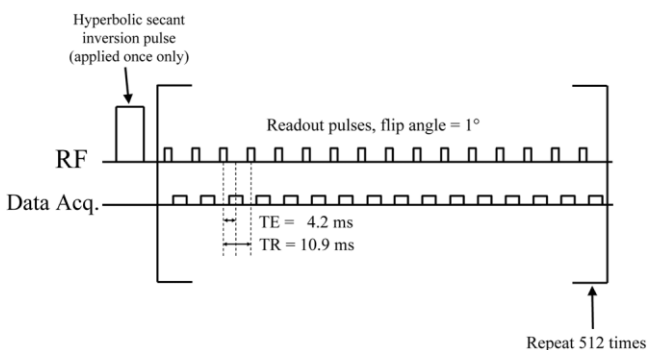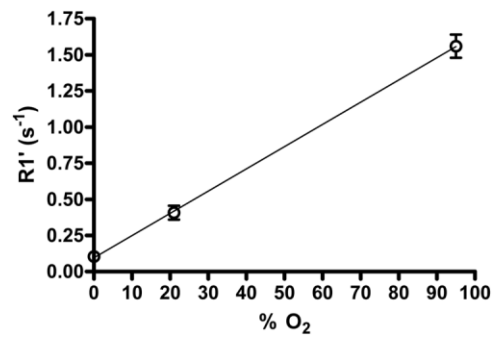

FIG. 2. Calibration (R_1') of HFB with respect to pO_2 (mmHg).

(tip diameter: 350 μm) were inserted using a 26G needle to make a track inside the tissue. Data were collected continuously at a sampling frequency of 0.1 Hz before, during, and after carbogen breathing. No change in temperature was observed during ^{19}F MR pulsing. OxyLite pO_2 measurements are single-point measurements; the volume sampled is confined to the sensor tip.

RESULTS

In Vitro Data

The respective R_1' measurements for HFB in 0, 21, and 95% O_2 were 0.105 ± 0.006 s^{-1}, 0.407 ± 0.048 s^{-1}, and 1.56 ± 0.08 s^{-1}, providing a calibration curve of R_1' = 0.1048 (± 0.0060) + [0.002000 (± 0.000105)] pO_2, where R_1' is in units of s^{-1} and pO_2 is in units of mmHg (Fig. 2). This is similar to the calibration curve found by Mason and colleagues (7), R_1 = 0.0835 (± 0.0010) + [0.001876 (± 0.000009)] pO_2. (The better precision reported by the Mason group is probably due to their larger number of calibration samples used.) The relation pO_2 = (R_1' − 0.1048)/0.002 was used voxel-by-voxel for the remainder of our experiments.

In Vivo Data

Tumor oxygenation was monitored simultaneously with ^{19}F MRI and OxyLite in TLT tumors before, during, and after a respiratory challenge with carbogen. The temperature was monitored during the experiments. Carbogen breathing is known to improve tumor oxygenation in experimental models. A typical result is shown in Fig. 3, with OxyLite and ^{19}F MRI measurements recorded for the same mouse. We can see that the dynamics of response are similar between the two techniques, but that the amplitude of response to carbogen inhalation is quite different despite similar baseline and postmortem values. During carbogen breathing the pO_2 measured by ^{19}F MRI was higher than that measured by OxyLite for the majority of experiments. This is illustrated in Fig. 4, where all values from both techniques are reported. Color pO_2 maps were created from the ^{19}F MRI data to investigate heterogeneity of response (Fig. 5). Histograms of the ^{19}F MRI data were also generated (Fig. 5). The color maps show that each region of the tumor responds differently to the respiratory challenge, with some groups of pixels having values above 100 mmHg. From the histograms we observe a clear shift to
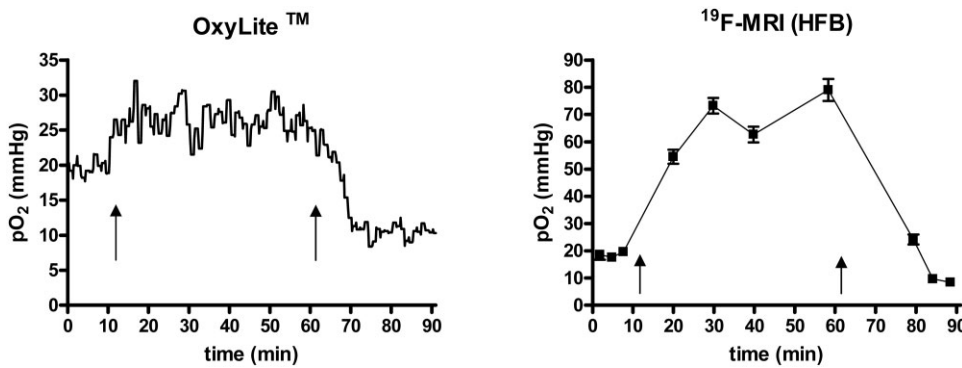

FIG. 1. Schematic description of the SNAP-IR pulse sequence.

FIG. 3. Comparison of the simultaneous monitoring of tumor oxygenation with OxyLite (single probe) (left) and ^{19}F MRI (mean pO_2) (right) (typical tumor). Arrows indicate the switch from air to carbogen (first arrow) or carbogen to air (second arrow). Note that the y scale (pO_2 in mmHg) is not similar for both techniques.

the right of the median pO_2 value under carbogen-breathing conditions. For most tumors (such as in Fig. 5) a bimodal distribution was observed for the carbogen breathing, reflecting the high heterogeneity of response of TLT tumors.

DISCUSSION

The SNAP-IR pulse sequence allowed us to sample tumor oxygenation with an effective in-plane spatial resolution

FIG. 4. Scatter graphs showing all individual and mean MRI pO_2 values under air, carbogen, and isoflurane 5% breathing conditions. Left: OxyLite (single probe). Right: ^{19}F MRI (mean pO_2).

(1.88 mm) similar to that of FREDOM (1.25 mm) (7). Our acquisition time was 1.5 min, which is shorter than that of FREDOM (6.5 min). For T_1 measurements it has been theorized that a Look–Locker (17) data acquisition strategy (e.g., SNAP-IR) provides nearly twice the T_1 measurement precision per unit acquisition time compared to a saturation-recovery data acquisition strategy (e.g., FREDOM). However, we did not investigate further this potential efficiency advantage of SNAP-IR over FREDOM. The extra signal-to-noise ratio obtained from the relatively high amount of HFB injected into the tumors ensured that the higher temporal resolution could be obtained without sacrificing precision.

Mean basal pO_2 values were quite variable from one tumor to another, ranging between 5 and 20 mmHg with both techniques. However, pO_2 maps and histograms obtained with ^{19}F MRI showed many regions of highly hypoxic pixels, which are the radiobiologically relevant regions. Tumor pO_2 measured with both techniques showed a consistent increase during the carbogen intervention. Our in vivo data corroborate with results obtained with previous ^{19}F MRI and OxyLite studies (18,19) as well as with other techniques, such as EPR oximetry or BOLD MRI (19,20), in terms of pO_2 changes under similar respiratory challenges. Indeed, changes in pO_2 from 20 to >100 torr in response to carbogen breathing have been reported in this tumor model, entirely in line with ^{19}F MRI measurements here. There is, however, a huge difference in the magnitude of response between the two techniques. The high heterogeneity of response might explain the lack of direct agreement between ^{19}F MRI and OxyLite. The sampling volumes of the two techniques are indeed very different. Moreover, for the ^{19}F MRI data there was always a small region of "high responding" pixels that had a huge influence on the mean and median values. The probability of inserting the probe at that very location was low. Results obtained with the fiber-optic probes were more similar to the "low responding" pixels observed with ^{19}F MRI, which are more numerous. Indeed, such voxels are apparent in the pO_2 maps in Fig. 5.

By combining three OxyLite probes simultaneously in the same tumor, Zhao et al. (18) were able to interrogate different tumor regions so as to examine baseline and dynamic responses of regions, which were hypoxic, of low oxygenation, and with high baseline oxygenation. This information would have been particularly relevant to the present study, although it would have been technically impossible to combine three probes within the sensitive
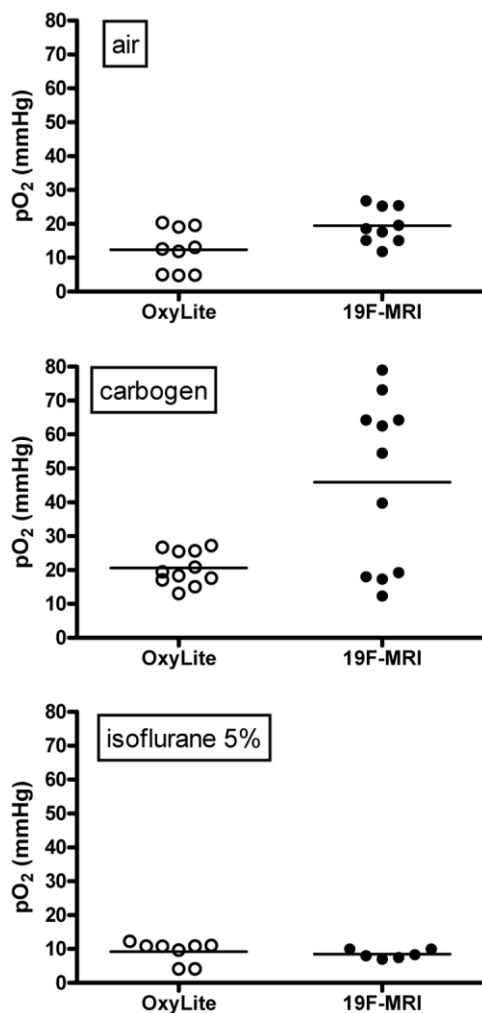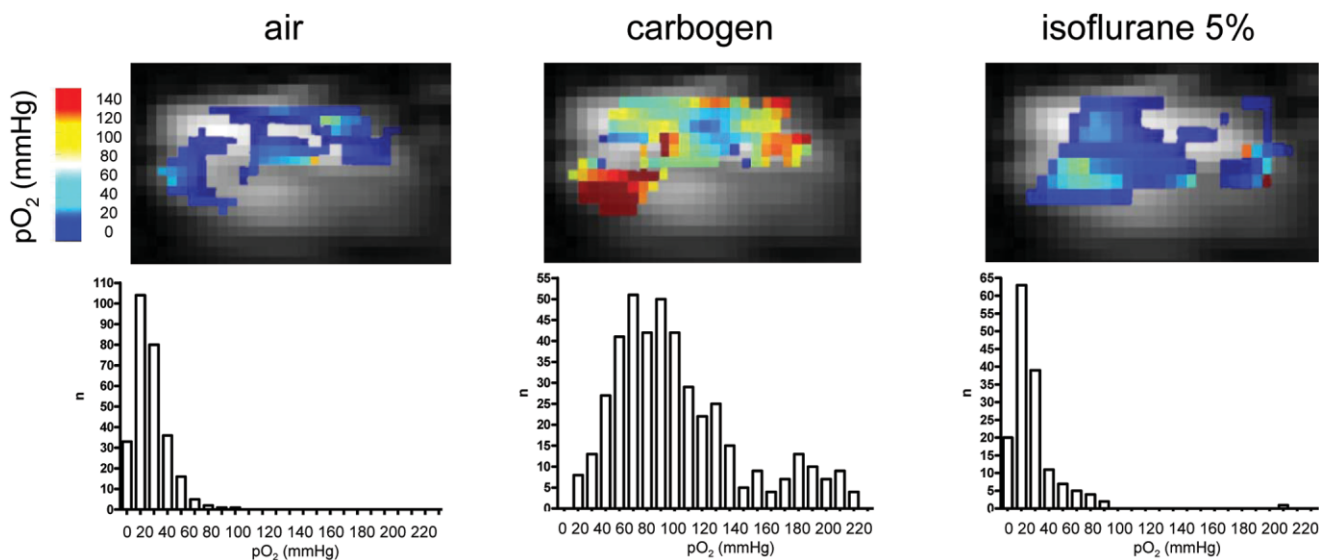
FIG. 5. Typical oxygen maps of a typical tumor under air, carbogen, and isoflurane 5% (sacrifice) breathing conditions and their corresponding histograms.

volume of the surface coil simultaneously with the ^{19}F measurements.

Finally, it has been described that the relationship of the OxyLite sensor response versus oxygen concentration is nonlinear (21). Therefore, errors in determining fluorescence lifetime are more serious at high oxygen concentrations (where the Stern–Volmer curve is flatter) than at low concentrations. This could explain why we only saw a modest increase in pO_2 in response to carbogen breathing with OxyLite in comparison with ^{19}F MRI.

Intratumoral injection of hexafluorobenzene has been argued to result in ^{19}F MRI oximetry interrogating poorly perfused, chronically hypoxic tumor regions (22). However, considering the distribution of the basal values in the current study, as well as the large response to carbogen breathing observed with ^{19}F MRI, we do believe that we interrogated both poorly perfused (chronically hypoxic) regions and well-perfused regions. Moreover, the role of acute hypoxia is now well recognized and this might explain why regions that seem completely hypoxic at one given time are still able respond to carbogen breathing.

It is possible, in principle, to correct the R_1' measurements to obtain R_1 values that would be measured from an unperturbed longitudinal relaxation recovery curve (16). This correction is given by $R_1 = R_1' + \ln[\cos(\alpha)] / TR$, where α is the flip angle and TR is the repetition time (spacing between RF pulses). The only effect that this correction would have on our data is that the intercept of the R_1 vs. pO_2 calibration curve would change from $0.1048 \pm 0.0060 \text{ s}^{-1}$ to $0.0908 \pm 0.0060 \text{ s}^{-1}$, putting it closer to Mason's $0.0835 \pm 0.0010 \text{ s}^{-1}$ (7). The correction would change neither the slope of the calibration curve nor the final pO_2 values estimated in vivo.

In conclusion, we present here a new ^{19}F MRI method for oxygen mapping using a SNAP-IR pulse sequence that is particularly relevant in terms of temporal resolution. We used the method to map tumor oxygenation in experimental tumors and showed the sensitivity of the technique to changes in tumor pO_2 with respect to respiratory challenges. Since the present sequence is more rapid then FREDOM, we suggest that it is particularly suitable to monitor acute changes of pO_2 in tumors.

REFERENCES

1. Vaupel P, Harrison L. Tumor hypoxia: causative factors, compensatory mechanisms, and cellular response. Oncologist 2004;9:4–9.
2. Gray L, Conger A, Ebert M, Hornsey S, Scott OC. The concentration of oxygen dissolved in tissues at time of irradiation as a factor in radiotherapy. Br J Radiol 1953;26:638–648.
3. Teicher BA, Holden SA, al-Achi A, Herman TS. Classification of antineoplastic treatments by their differential toxicity toward putative oxygenated and hypoxic tumor subpopulations in vivo in the FSaIIC murine fibrosarcoma. Cancer Res 1990;50:3339–3344.
4. Littlewood TJ. The impact of hemoglobin levels on treatment outcomes in patients with cancer. Semin Oncol 2001;28:49–53.
5. Tatum JL, Kelloff GJ, Gillies RJ, Arbeit JM, Brown JM, Chao KS, Chapman JD, Eckelman WC, Fyles AW, Giaccia AJ, Hill RP, Koch CJ, Krishna MC, Krohn KA, Lewis JS, Mason RP, Melillo G, Padhani AR, Powis G, Rajendran JG, Reba R, Robinson SP, Semenza GL, Swartz HM, Vaupel P, Yang D, Croft B, Hoffman J, Liu G, Stone H, Sullivan D. Hypoxia: importance in tumor biology, noninvasive measurement by imaging, and value of its measurement in the management of cancer therapy. Int J Radiat Biol 2006;82:699–757.
6. Gallez B, Baudelet C, Jordan BF. Assessment of tumor oxygenation by electron paramagnetic resonance: principles and applications. NMR Biomed 2004;17:240–262.
7. Hunjan S, Zhao D, Constantinescu A, Hahn EW, Antich PP, Mason RP. Tumor oximetry: demonstration of an enhanced dynamic mapping procedure using fluorine-19 echo planar magnetic resonance imaging in the Dunning prostate R3327-AT1 rat tumor. Int J Radiat Oncol Biol Phys 2001;49:1097–1108.
8. Mason RP, Hunjan S, Constantinescu A, Song Y, Zhao D, Hahn EW, Antich PP, Peschke P. Tumor oximetry: comparison of 19F MR EPI and electrodes. Adv Exp Med Biol 2003;530:19–27.
9. Zhao D, Constantinescu A, Chang CH, Hahn EW, Mason RP. Correlation of tumor oxygen dynamics with radiation response of the dunning prostate R3327-HI tumor. Radiat Res 2003;159:621–631.
10. Zhao D, Jiang L, Mason RP. Measuring changes in tumor oxygenation. Methods Enzymol 2004;386:378–418.
11. Xia M, Kodibagkar V, Liu H, Mason RP. Tumour oxygen dynamics measured simultaneously by near-infrared spectroscopy and 19F magnetic resonance imaging in rats. Phys Med Biol 2006;51:45–60.

12. Taper H, Woolley GW, Teller MN, Lardis MP. A new transplantable mouse liver tumor of spontaneous origin. Cancer Res 1966;26:143–148.

13. Hoehn-Berlage M, Norris D, Bockhorst K, Ernestus RI, Kloiber O, Bonnekoh P, Leibfritz D, Hossmann KA. T1 snapshot FLASH measurement of rat brain glioma: kinetics of the tumor-enhancing contrast agent manganese (III) tetraphenylporphine sulfonate. Magn Reson Med 1992;27:201–213.

14. Blüml S, Schad LR, Stepanow B, Lorenz WJ. Spin-lattice relaxation time measurement by means of a TurboFLASH technique. Magn Reson Med 1993;30:289–295.

15. Laukemper-Ostendorf S, Scholz A, Bürger K, Heussel CP, Schmittner M, Weiler N, Markstaller K, Eberle B, Kauczor HU, Quintel M, Thelen M, Schreiber WG. 19F MRI of perflubron for measurement of oxygen partial pressure in porcine lungs during partial liquid ventilation. Magn Reson Med 2002;47:82–89.

16. Look DC, Locker DR. Time saving in measurement of NMR and EPR relaxation times. Rev Sci Instrum 1970;41:250–251.

17. Crawley AP, Henkelman RM. A comparison of one-shot and recovery methods in T1 imaging. Magn Reson Med 1988;7:23–34.

18. Zhao D, Constantinescu A, Hahn EW, Mason RP. Tumor oxygen dynamics with respect to growth and respiratory challenge: investigation of the Dunning prostate R3327-HI tumor. Radiat Res 2001;156:510–520.

19. Baudelet C, Gallez B. How does blood oxygen level-dependent (BOLD) contrast correlate with oxygen partial pressure (pO2) inside tumors? Magn Reson Med 2002;48:980–986.

20. Jordan BF, Gregoire V, Demeure RJ, Sonveaux P, Feron O, O'Hara J, Vanhulle VP, Delzenne N, Gallez B. Insulin increases the sensitivity of tumors to irradiation: involvement of an increase in tumor oxygenation mediated by a nitric oxide-dependent decrease of the tumor cells oxygen consumption. Cancer Res 2002;62:3555–3561.

21. Griffiths JR, Robinson SP. The OxyLite: a fibre-optic oxygen sensor. Br J Radiol 1999;72:627–630.

22. McIntyre DJO, McCoy CL, Griffiths JR. Tumour oxygenation measurements by 19F MRI of perfluorocarbons. Curr Sci 1999;76:753–762.